Journal of Sol-Gel Science and Technology (2023) 105:370–387
https://doi.org/10.1007/s10971-022-06016-3

ORIGINAL PAPER: FUNDAMENTALS OF SOL-GEL AND HYBRID MATERIALS PROCESSING

Rapid synthesis of MCM-41 and SBA-15 by microwave irradiation: promising adsorbents for CO_2 adsorption

Marília R. Oliveira[1,2,3] · Juan A. Cecilia[3] · Juliana F. De Conto[1] · Silvia M. Egues[1,2] · Enrique Rodríguez-Castellón[3]

Received: 24 October 2022 / Accepted: 7 December 2022 / Published online: 31 December 2022

Abstract

It is known that the world scenario is one of constant search for sustainable technologies that can reduce the emission of carbon dioxide (CO_2) in the atmosphere. This is because CO_2 is seen as the main responsible for the increase in the generation of greenhouse gases, which leads to global warming and climate change. The development of efficient adsorbents for CO_2 capture is a current challenge. MCM-41 and SBA-15 were synthesized in a microwave reactor and used as adsorbents in this work. Microwave irradiation presents itself as an easy synthesis strategy with less preparation time and energy requirement. The silica synthesis period was extremely reduced (1 h) at a temperature of 60 and 80 °C in the microwave reactor, obtaining silica with good textural and chemical properties. The CO_2 adsorption isotherms were performed at 0, 25, and 40 °C at 1 bar. The MCM-41 and SBA-15 present favorable results for CO_2 capture processes, showing that pure silica synthesized by microwave already obtains promising results, reaching a maximum adsorption capacity of 2.16 mmol g^{-1} (1 bar—0 °C) and a good fit for the Langmuir, DsL and Toth models. Furthermore, to increase CO_2 adsorption, the mesoporous silica was also modified via impregnation with branched polyethylene diamine (PEI) or tetraethylenepentamine (TEPA). It is worth mentioning that microwave irradiation reduced the synthesis steps and improved the properties and adsorption capacity of the silica. This work opens new opportunities in the efficient preparation of materials that require optimizing the adsorbent synthesis process.

Supplementary information The online version contains supplementary material available at https://doi.org/10.1007/s10971-022-06016-3.

✉ Enrique Rodríguez-Castellón
castellon@uma.es

[1] Center for Studies in Colloidal Systems (NUESC), Laboratory of Materials Synthesis and Chromatography (LSINCROM), Institute of Technology and Research (ITP), Av. Murilo Dantas, 300, Aracaju, SE 49032-490, Brazil

[2] Postgraduate Programme in Process Engineering, Tiradentes University (UNIT), Av. Murilo Dantas, 300, Aracaju, SE 49032-490, Brazil

[3] Department of Inorganic Chemistry, Crystallography, and Mineralogy, Faculty of Sciences, University of Málaga, Avda. Cervantes, 2, 29071 Málaga, Spain

Graphical Abstract

CO_2 adsorption capacity of MCM-41 and SBA-15 prepared by rapid synthesis using microwave irradiation and amino functionalized.

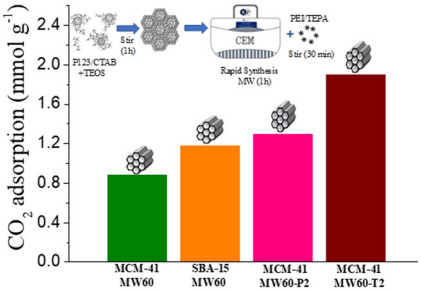

Keywords Rapid synthesis · SBA-15 · MCM-41 · Microwave · CO_2 adsorption

Highlights

- MCM-41 and SBA-15 were synthesized in 1 h at 60 and 80 °C by microwave irradiation.
- Heating by microwave irradiation is an efficient tool to be used in the synthesis of silica.
- Pure silicas synthesized by microwave irradiation are promising adsorbents for CO_2 adsorption.
- The CO_2 adsorption capacity of silicas decreases with increasing temperature.

1 Introduction

The burning of fossil fuels is one of the main causes of greenhouse gas emissions with the release of CO_2 being a global concern due to its impact on the climate. Thus, many studies are being developed to generate technologies to reduce these emissions [1, 2]. Among the existing methods, CO_2 capture by adsorption is presented as an efficient method, due to its high adsorption capacity, as well as its simplicity and low cost [3, 4]. The development of a suitable adsorbent is the most important component for adsorption [5]. Many studies report that to obtain an efficient CO_2 capture, the adsorbent must have high CO_2 adsorption capacity and selectivity, low cost of raw materials, a moderate pore diameter with a high surface area, and good thermal and hydrothermal stability [6, 7].

Thus, the search for adsorbents that are competitive for this process has led several researchers to design different materials. Mesoporous and microporous silica, activated carbons, zeolites, MOFs, and amine-modified materials make up the main class of adsorbents used for CO_2 adsorption [1, 8–10]. In 1992, the first family of ordered silicas, called M41S, was reported by scientists at Mobil Oil Corporation. Since their discovery, ordered mesoporous silicas such as MCM-41 and SBA-15 have attracted much attention from the scientific community due to their structural and physicochemical properties, such as high surface area and defined pore volume. The MCM-41 and SBA-15 silicas have an ordered pore arrangement, a surface area between 600 and 1300 $m^2 g^{-1}$ and a pore diameter between 2 and 30 nm [11, 12].

Cecilia et al. [13] synthesized pure hollow silica microspheres and functionalized with aminopropyltriethoxysilane (APTES), and via impregnation with polyethylenimine (PEI) or tetraethylenepentamine (TEPA), where it was possible to obtain high surface area and homogeneous pore size distribution. Impregnation with amine polymers, such as PEI and TEPA, was more efficient for adsorbents with greater external surface area. The incorporation of TEPA molecules increased the dispersion of the amine species mainly at high loads. The CO_2 adsorption isotherms of the amine-functionalized silicas were fitted to the Dual-Langmuir model, where the physical and chemical adsorption sites are described. The stability of the adsorbents was also evaluated, where the silicas showed resistance of the amine species to the regeneration conditions, at least after five cycles. Muchan et al. [7] synthesized pure MCM-41 and SBA-15 silicas and modified with APTES for application in CO_2 adsorption. The modified silicas showed good performance stability after five cycles of adsorption/desorption. The CO_2 adsorption capacity of the mesoporous silicas depends on the number of amine sites and the pore volume. Thus, for the amine-modified silica, the adsorption capacity increased from 0.63 to 1.01 mmol g^{-1} for MCM-41 silica and from 0.71 to 1.75 mmol g^{-1} for SBA-15 silica. It is worth mentioning that the pore diameter and the porous structure of the adsorbent also affect the adsorption of CO_2, and it is also possible to obtain good results with pure silica,

just by modifying some parameters in the synthesis step. Furthermore, the functionalization with APTES depends on the amount of silanol groups of the porous silica MCM-41 and SBA-15, since the grafting of APTES occurs with the silanol groups.

It is known that silica has already been recognized as a powerful adsorbent, as it has been used for decades until today, and its properties such as stability, superficial area, pore volume and versatility, the possibility of modifying the silica surface according to hydrophilicity or hydrophobicity make it a promising adsorbent for process adsorption [14–16]. Furthermore, it is important to note that ordered mesoporous silicas perform well in terms of their mechanical stability, being able to be used in different pressure ranges [17], thus presenting desired properties for their use in pressurized systems. Mayanovic et al. [18] evaluated the thermal, mechanical, and hydrothermal properties of mesoporous silicas under different pressure and temperature conditions. Silica SBA-15 showed excellent hydrothermal stability for supercritical conditions (500 °C and 3700 bar) and it is still possible to improve this property by varying the types of precursors in the synthesis step or making changes to its surface. In addition, the development of new synthesis routes, such as the use of microwave irradiation (MW), generates advantages over conventional synthesis to obtain this material, reducing the use of solvents, reaction time, and energy. It is worth mentioning the reduction in the use of solvents and energy, since it is a faster process when compared to the synthesis using autoclave [16, 19].

Heating by microwave irradiation is an efficient tool to be used in the synthesis of silicas and that, in addition to reducing the reaction time, it is also possible to provide greater uniformity in the pores of the materials. The use of MW in silica synthesis processes has already been used in several processes. Peres et al. [20] synthesized silica nanoparticles through rice husk using microwave heating at a temperature of 80 °C and 30 min. The authors concluded that microwave synthesis generated material with greater purity, surface area, pore volume and porosity in less time compared to the traditional method. This is because, compared to conventional methods, microwave heating is rapid volumetric heating without the conductive heat process, which can achieve uniform heating in a short time. Oliveira et al. [16] showed that microwave irradiation in the synthesis of SBA-15 silica reduced the synthesis time, making it possible to control the textural properties, in addition to obtaining silicas with a greater amount of silanol groups when compared to silicas synthesized in an autoclave. Bordoni et al. [21] used microwave irradiation to expand the pores of non-calcined SiO_2-based mesoporous materials (core-shell nanoparticles and SBA-15). Using a greener alternative, the authors chose pore-broadening agents (mesitylene and naphthalene) over common surfactants for the synthesis step and demonstrated that the use of microwaves significantly decreased the reaction time, and it was compatible with pore models of ionic and non-ionic surfactants. Furthermore, the microwave post-treatment of the calcined mesoporous materials with pore dilating agents allowed the control and increase of the final pore dimensions of the material as well as the adaptation of the molecular structure of the materials.

However, the use of silicas synthesized by microwave irradiation, without modification/impregnation of amines for the adsorption of CO_2 is a subject little discussed in the scientific community. You et al. [22] evaluated the CO_2 adsorption capacity of zeolite Beta synthesized by MW (Beta-MW) and by the conventional hydrothermal method (Beta-HT). The CO_2 adsorption tests were investigated at a temperature of 40 °C and absolute pressure of 1 bar. Beta-MW was rapidly synthesized in 4 h ($S_{BET} = 463\ m^2\ g^{-1}$ and $Vp = 0.28\ cm^3\ g^{-1}$), obtaining properties like Beta-HT in 48 h ($S_{BET} = 483\ m^2\ g^{-1}$ and $Vp = 0.29\ cm^3\ g^{-1}$). However, Beta-MW obtained better adsorption capacity ($2.16\ mmol\ g^{-1}$) and CO_2 selectivity (17.1 %) than Beta-HT ($1.94\ mmol\ g^{-1}$ and 14.5%). This result showed efficiency in the synthesis of the adsorbent per MW and was attributed to the best hydrophilicity generated in the synthesis per MW.

In this way, it will be shown that it is also possible to obtain promising results with pure silica, just by modifying the synthesis route. Given the adsorbents already mentioned in the literature, this interest in ordered mesoporous silica is attributed to its easy handling, affordable cost when compared to other adsorbents, silanol groups that have great interaction with CO_2 and its physicochemical properties, such as adjustable pore size, high surface area, good stability, and low density [16, 23, 24]. In this context, the idea of this study was to evaluate the textural and structural properties of MCM-41 and SBA-15 mesoporous silicas synthesized by microwave irradiation and the efficiency of CO_2 adsorption.

2 Materials and methods

2.1 Materials

MCM-41 synthesis was carried out using cetyltrimethylammonium bromide (CTAB) (98%, Sigma-Aldrich) as a template, tetraethylorthosilicate (TEOS) (Sigma-Aldrich, 98%) as silicon source, and aqueous ammonia solution (25% Merck). SBA-15 synthesis was carried out using Pluronic P123, (Sigma-Aldrich) as template, TEOS as silicon source, and hydrochloric acid (HCl) (Vetec, 37%). The microwave reactor used in the silica synthesis was the CEM, Discovery SP model, single-mode type, with temperature and power control.

2.2 MCM-41 synthesis

MCM-41 synthesis was adapted from the procedure described by Grun et al. [25] and Oliveira et al. [16]. First, 1.4 g of CTAB were dissolved in 60 ml of deionized water, under stirring, at a temperature of ≅ 25 °C. Then, 4.75 g of aqueous ammonia solution was added to the reaction. While stirring, 5 g of TEOS were slowly added to the solution. The mixture was stirred for 1 h at a temperature of ≅ 25 °C, after which it was poured into a quartz tube and placed in the microwave. The reaction temperature and time used in the microwave synthesis were 60 and 80 °C for 1 h, maximum power of 250 W (CEM, Discovery SP model). The obtained adsorbents were washed with deionized water, filtered under vacuum, and dried in an oven at 80 °C for 8 h. Then, the adsorbents were calcined for 6 h at 550 °C (10 °C min $^{-1}$) to remove the CTAB surfactant. The samples were named MCM-41-MW60 and MCM-41-MW80.

2.3 SBA-15 synthesis

The synthesis of SBA-15 followed the procedure described by Oliveira et al. [16]. In brief, 2 g of copolymer P123 were dissolved in a beaker containing 75 ml of HCl solution (2 M). The mixture was kept at 40 °C under constant stirring until P123 was dissolved. In total, 4.55 ml of TEOS were then slowly added to the system. The system was maintained for another 1 h under the same conditions. Then, the mixture was transferred to a quartz tube and introduced into a microwave CEM reactor and the same conditions of synthesis of silica MCM-41 were used (60 and 80 °C for 1 h). The white solid obtained was filtered, washed with deionized water, dried, and calcined under the same conditions of MCM-41. The samples were named SBA-15-MW60 and SBA-15-MW80.

2.4 Modification of the silicas with amine groups

The modification by impregnation was carried out following the methodology proposed by Xu et al. [26]. and Cecilia et al. [27]. For each impregnation, 0.3 g of silica were dried at 110 °C overnight, and then, the dried solid was added to a solution of methanol/amine-rich polymer (PEI or TEPA). The mass ratio methanol/ silica was maintained constant at 8:1 for each sample, while the methanol/PEI ratio was varied in each case. The desired amount of amine (25, 40, 55, or 70% by mass) was weighed in a beaker and then dissolved in methanol under stirring for 10 min. Then, the silica was added to the amino/methanol solution. The resulting suspension was continuously stirred for 30 min. Then the suspension was dried in an oven at 80 °C for 24 h. The samples were labeled as MCM-41-MW60-XY, where x is the amine type and y is the amine content, being 25% equivalent to 1, 40% to 2, 55% to 3 and 70% to 4. For example, silica modified with 25% of PEI will be called MCM-41-MW60-P1. The silica modified with 55% of TEPA will be called MCM-41-MW60-T3.

2.5 Characterization techniques

Nitrogen adsorption/desorption measurements were performed at liquid N_2 temperature (−196 °C) with an ASAP 2420 apparatus from Micromeritics. The specific surface area was determined by the Brunauer-Emmett-Teller equation (BET) and Langmuir using the adsorption data in the range of relative pressures of 0 to 1 bar. The pore size distribution was determined from the desorption branch of the isotherm using the non-local density functional theory (NLDFT) and MP method. The total pore volume was calculated from adsorbed N_2 at a relative pressure $(P/P_0) = 0.99$. Before the measurements, samples were outgassed overnight at 120 °C and 10^{-4} mbar.

The elemental chemical analysis was determined using a CHNS EA3000 analyzer through the combustion of the samples at 1100 °C in pure oxygen.

XPS studies were conducted on a Physical Electronic PHI 5700 spectrometer using non-monochromatic Mg Kα radiation (300 W, 15 kV, 1253.6 eV). The core level signals of C 1*s*, O 1*s*, and Si 2*p* were analyzed with a hemispherical multichannel detector. The BE values were referenced to the C 1*s* signal of adventitious carbon (284.8 eV). The absolute error in the binding energies values of high resolution spectra is ±0.1 eV, as indicated by the manufacturer (Physical Electronics); binding energies values within 0.2 eV can be considered the same, within the experimental error. The error in determination of the atomic concentration % was below 5%.

^{29}Si MAS-NMR (magic angle spinning nuclear magnetic resonance) spectra were recorded at RT in an AVANCEIII HD 600 (Bruker AXS) spectrometer using a double resonance DVT probe of 4.0 mm at a spinning rate of 13 kHz. ^{29}Si MAS NMR spectra were recorded with a 8-ms 90° pulse and 60-s delay with ^{1}H decoupling (^{29}Si Hpdec with cw decoupling sequence for Si) and summing up 1000 scans.

The Fourier Transform Infrared (FTIR) spectra were collected in a Vertex70 (Bruker) FTIR spectrometer equipped with a Golden Gate Single Reflection Diamond ATR System accessory. For the acquisition of the spectra, a standard spectral resolution of 4 cm^{-1} was used in the spectral range of 4000–500 cm^{-1}, as well as 64 accumulations.

X-ray powder diffraction patterns (XRD) were collected on a PANanalytical EMPYREAN automated diffractometer. Powder patterns were recorded in theta-theta transmission configuration emplacing the sample between two kapton foils

and by using a focusing mirror and the PIXcel 3D detector (working in 1D mode) with a step size of 0.013° (2θ). The powder patterns were recorded between 0.5 and 10 degrees in 2θ with a total measuring time of 60 min. The porous structures was analyzed by transmission electron microscope (TEM—FEI Talos F200X).

2.6 Adsorption CO_2

The adsorption tests were used to evaluate the CO_2 capture capacity of the silica. Adsorption/desorption isotherms were measured with a Micromeritics ASAP 2020 Analyzer (i.e., volumetrically) at 0, 25, and 40 °C, all under absolute pressure ranging to 1 bar. The purity of the CO_2 used in the tests was 99.998%. Before the measurements, samples were outgassed at 110 °C and 10^{-4} mbar.

2.7 Adsorption models

The CO_2 adsorption isotherms on silicas were fitted by using the Langmuir (1) and Toth models (3) [28]. The Langmuir equation is:

$$q_i = q_m \frac{bP}{1 + bP} \tag{1}$$

where q_i is the adsorbed amount of component i; q_m is the maximum adsorption capacity of the adsorbent; b is the adsorption constant or the Langmuir constant; P is the pressure. The dependence on the Langmuir constant temperature is expressed by the Van't Hoff equation:

$$b_i = b_i^0 e^{\left(\frac{-\Delta H}{RT}\right)} \tag{2}$$

where K_i is the adsorption constant at infinite temperature; $(-\Delta H)$ is the heat of adsorption on the homogeneous surface; R is the universal gas constant; and T is the system temperature in Kelvin.

To describe isotherms of amine-modified materials, the Dualsite Langmuir (DsL) model was used, to distinguish between contributions due to chemical reactions and physical interactions. The DsL equation is:

$$q_i = q_{m,1} \frac{b_1 \times P}{1 + b_1 \times P} + q_{m,2} \frac{b_2 \times P}{1 + b_2 \times P} \tag{3}$$

where q_i is the adsorbed amount of component i; q_{m1} and q_{m2} are the maximum adsorption capacity of the adsorbent; b_1 and b_2 are the adsorption constant or the Langmuir constant; P is the pressure.

The Toth isotherm model was developed in 1961 to produce a better fit when compared to empirical equations such as Langmuir, DSL, SIPS. Toth's equation allows a good description of many systems with sub-monolayer coverage [28]. Toth's isothermal equation is:

$$q_i = q_{m,i} \frac{K_i \times P}{\left[1 + (K_i \times P)^{n_i}\right]^{\frac{1}{n_i}}} \tag{4}$$

where q_i and $q_{m,i}$ are the amount adsorbed and the maximum adsorption capacity of component i; K_i and n_i are specific parameters for adsorbate-adsorbent pairs; P is the pressure. For $n = 1$, the Toth isotherm reduces to the Langmuir equation. As n deviates further from unity, the system is more heterogeneous. This isotherm assumes that the adsorption occurs in only one layer and allows the interaction between the adsorbed molecules.

2.8 Thermodynamic parameters

Thermodynamic parameters can be used to assess whether the sorption process was spontaneous or not in the behavior of adsorbents. Equation van't Hoff (5) was used for calculation of enthalpy and entropy from the slope and intercept of plot $\ln K$ vs. $1/T$:

$$\ln K^0 = \frac{\Delta S^0}{R} - \frac{\Delta H^0}{RT} \tag{5}$$

where R is the universal gas constant (8.314 J mol^{-1} K^{-1}), T is the absolute temperature (K).

The standard Gibbs free energy change can be calculated by Eq. (6):

$$\Delta G = -RT \ln K^0 \tag{6}$$

2.9 Stability between adsorption cycles

To evaluate the efficiency of the adsorbents in successive cycles of adsorption, reuse tests were carried out. CO_2 adsorption capacities were obtained at 1 bar for the silicas with the best results, i.e., MCM-41-MW60 and SBA-15-MW60. The reuse test was repeated three times for each adsorbent. The temperature selected to measure the CO_2 capacity was 25 °C. Between the adsorption/desorption runs, the silicas were isothermally degassed for 4 h.

3 Results and discussion

3.1 Characterization

N_2 adsorption/desorption isotherms at −196 °C for the mesoporous silicas are shown in Fig. 1. Recalling that the silicas synthesized at 60 °C are called MW60 and at 80 °C as MW80. The N_2 adsorption/desorption analysis of the MCM-41 and SBA-15 silicas showed Type IV isotherms,

being Type IV(a) for silicas MCM-41-MW60 and MCM-41-MW80, since the adsorption and desorption branches do not fully combine, where the adsorption in the mesopores is determined by the interactions between the adsorbent and the adsorbate and by the capillary condensation, which presents hysteresis of the type H4 [29].

Silica SBA-15-MW80 also has a type IV(a) isotherm, which is suggested when the isotherms do not reach a well-defined saturation plateau, presenting a behavior close to an S-shaped isotherm [30]. However, its hysteresis loop is of the H2(b) type, which is associated with pore blockage or pore narrowing and can be observed in some ordered silicas after hydrothermal treatment. For SBA-15-MW60, an excess has occurred, where the Type I(b) isotherm is noted, showing that adsorption and desorption are fully compatible, pore size distributions in a wider range, including larger sized micropores and possibly narrow mesopores (<2.5 nm) [29]. It is believed that for this sample, during microwave irradiation, there was a blockage of the pores on the surface of the silica, presenting only micropores on its surface, which is unusual for SBA-15 silica, however, Oliveira et al. [16] showed in his work that it was possible to obtain mesoporous silica at a temperature of 60 °C.

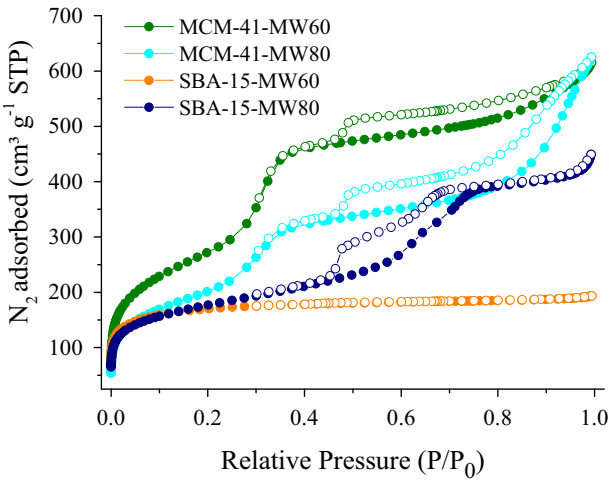

Fig. 1 N_2 adsorption/desorption isotherms at –196 °C for the MCM-41-MW60, MCM-41-MW80, SBA-15-MW60, and SBA-15-MW80

The pore size distribution curves were obtained by the NLDFT and MP method and are shown in Fig. 2, where it is possible to analyze the micro and mesopore regions. MCM-41 type samples have a narrower pore distribution than SBA-15 type silica. The microporosity of silicas decreases with increasing temperature used in the microwave reactor, as reported by Galarneau et al. [31] that using the higher aging temperature moves the surfactant micelles away from each other, causing the intercommunication between them to decrease. However, to silica SBA-15-MW60 has a predominant micropore region, which is best visualized in Fig. 2b and with the data from Table 1, where a surface area (S_{BET}) of 788 $m^2\,g^{-1}$ and a micropore area (S_{mp}) of 749 $m^2\,g^{-1}$ are verified, showing the predominance of micropores, which may be associated with a blockage of pores on the surface of this sample. According to Thommes et al. [29], this has already been noticed in some micro-mesoporous silicas, zeolites, and activated carbon, and reports that these phenomena occur if large pores have access to the external surface only through narrow

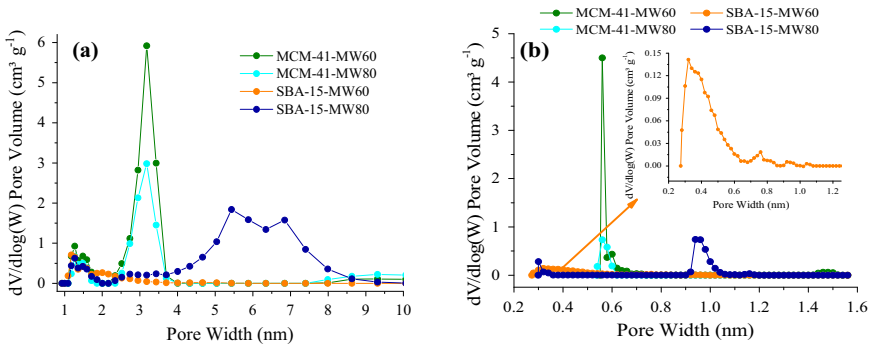

Fig. 2 Pore size distributions obtained by NLDFT (**a**) and MP (**b**) method for the studied adsorbents

Table 1 Textural properties of the obtained materials and atomic concentration % determined by XPS

Samples	S_{BET} ($m^2\,g^{-1}$)	$S_{mp\ t\text{-}plot}$ ($m^2\,g^{-1}$)	Vp ($cm^3\,g^{-1}$)	$V_{mp\ t\text{-}plot}$ ($cm^3\,g^{-1}$)	Dp_{DFT} (nm)	Dp_{MP} (nm)	XPS %C	%O	%Si
MCM-41-MW60	999	781	0.89	0.59	3.71	0.60	5.59	66.1	28.3
MCM-41-MW80	744	492	0.84	0.36	3.25	0.56	6.49	65.4	28.1
SBA-15-MW60	788	749	0.29	0.25	2.81	0.39	3.90	68.0	28.1
SBA-15-MW80	626	164	0.64	0.06	4.06	0.89	6.10	67.1	26.8

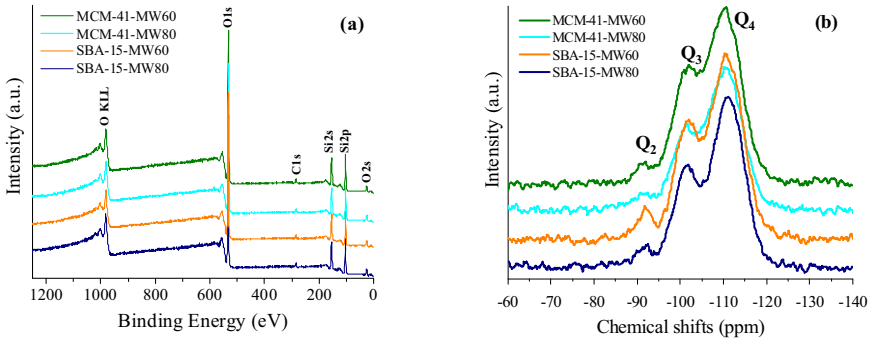

Fig. 3 XPS survey spectra (**a**) and ^{29}Si NMR spectra (**b**) for MCM-41-MW60, MCM-41-MW80, SBA-15-MW60, and SBA-15-MW80

bottlenecks. The pores are filled as before and remain filled during desorption until the narrow necks empty at lower vapor pressures.

Table 1 presents data on the textural properties of silica. The silicas synthesized at a temperature of 60 °C, presented higher surface area and pore volume values than the silicas synthesized at 80 °C, showing that it is possible to obtain silica with good textural properties at lower temperature conditions. In addition, it is noted that with only 1 h of hydrothermal treatment, it was possible to obtain silicas with surface area values and pore volumes very close to silicas synthesized in an autoclave, with a hydrothermal treatment of 24 h or even higher [16].

Rao et al. [32] synthesized MCM-41 silica for CO_2 adsorption using a 96 h hydrothermal treatment and obtained a surface area of 992 $m^2 g^{-1}$ and pore volume of 0.69 $cm^3 g^{-1}$. Muchan et al. [7] used MCM-41 and SBA-15 silica for CO_2 adsorption and performed the silica synthesis with a hydrothermal treatment of 12 and 24 h, obtaining a surface area of 1007 and 731 $m^2 g^{-1}$ and pore volume of 0.94 and 1.24 $cm^3 g^{-1}$, respectively. In the studies mentioned above, the synthesis of silica required more reaction time and, even so, surface areas lower than those of this work were obtained. This happens because microwave irradiation presents faster and more homogeneous heating, due to this, the hydrothermal treatment in microwave reactor ends up being faster and more efficient when compared to the hydrothermal process in the autoclave, thus reducing the synthesis time and maintaining the textural and structural properties of the samples [16].

The chemical composition of these materials was evaluated by XPS and NMR. MCM-41 and SBA-15 silicas are mesoporous materials with oxygen and silicon functional groups. Their atomic concentration is ~5% carbon, 67% oxygen and 28% silicon, according to the data obtained. The XPS spectrum of pure silicas contains three main photoemission signals, O 1*s*, Si 2*s*, and Si 2*p* (Fig. 3a). In addition to these, a carbon signal (C 1*s*) with a relatively low atomic percentage is also observed, which is associated with adventitious carbon. According to Yamashita and Hayes [33], carbon is always present in XPS analyses, as it is common to use its peak (carbon binding energy (BE) 284.6 eV) as a reference for the correction of other energies. The BE of the Si 2*p* signal in all samples was approximately at 103.6 eV, characteristic of mesoporous silicas such as MCM-41 and SBA-15. Furthermore, a single peak centered at 532.8 eV would be attributed to the photoemission of O 1*s*, attributed to the oxygen atoms of the siliceous support [34].

In Fig. 3b, it is also possible to analyze the ^{29}Si NMR spectra of the MCM-41 and SBA-15 silicas, which shows the three signals. The one with the greatest chemical shift, Q_4, refers to the silicon atoms located inside the inorganic network (siloxanes), linked to four structural oxygen atoms. The second signal, Q_3, is equivalent to surface silicon atoms bonded to a hydroxyl group (free silanols) and three structural oxygen atoms. The third, smaller chemical shift signal, Q_2, is attributed to surface silicon atoms bonded to two hydroxyl groups (geminal silanols) and two structural oxygen atoms [35].

The ordering and structure of the silica channels was confirmed using TEM and XRD. Figure 4 shows the formation of the aligned and hexagonal channels, characteristic of these ordered silicas. Note that there was no expressive difference in the structures of MCM-41 and SBA-15 with the temperature variation of 60 and 80 °C. It is also verified the configuration in the form of equidistant parallel lines in the mesoporous silicas, except for the SBA-15-MW60 silica. Chaignon et al. [36] synthesized mesoporous silicas of the MCM-41 type using microwave irradiation and evaluated the effect of temperature (150 and 180 °C) on the synthesis process. The authors found that the proper use of microwave irradiation not only reduces the synthesis time of mesoporous silicas but when combined with programmed temperatures it is also possible to obtain ordered materials with consolidated structures and good thermal stability when compared to materials obtained by the hydrothermal process conventional using autoclave.

The XRD patterns characteristic of the MCM-41 mesoporous silica present 3 to 4 peaks, referring to the reflection planes (100), (110), (200) and (210), with the (100) plane being the most intense [11]. These peaks are the reference

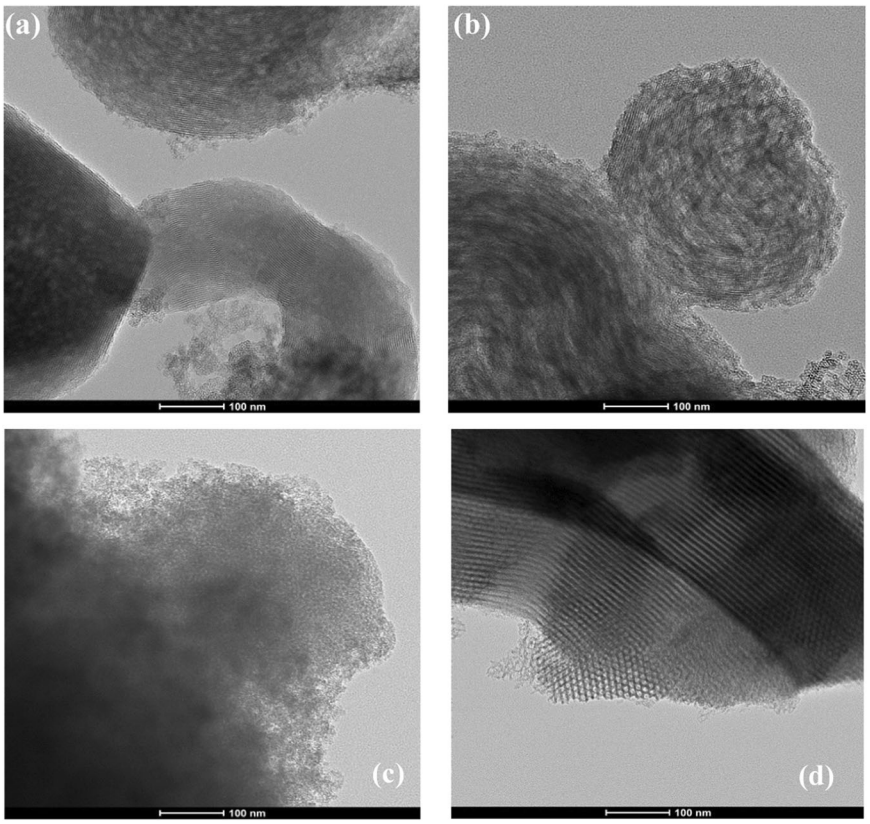

Fig. 4 TEM micrographs of **a** MCM-41-MW60, **b** MCM-41-MW80, **c** SBA-15-MW60, and **d** SBA-15-MW80

of the hexagonal unit cell of the material. In Supplementary Material (Fig. 13) can be seen in that MCM-41 silicas present all peaks, while for SBA-15 silica, the main peak referring to the (100) plane, which characterizes ordered mesoporous materials, is only noticed for SBA-15-MW80, corroborating the results obtained by the adsorption/desorption of N_2. In addition to pore blockages on the surface, this may also be related to the formation of "hot spots" during microwave radiation, which may have influenced the disordering of SBA-15-MW60 [16]. Through chemical composition analysis, this sample presented similar results to the others, however it was proven that it does not present the typical order of the SBA-15.

Even with the unexpected result for SBA-15-MW60 silica, all silicas will be applied in CO_2 adsorption, to evaluate these properties. Furthermore, it is worth mentioning that microwave irradiation is a fast and adequate technique that allows adapting the porous and surface structure of a material, in addition to generating new opportunities for obtaining pure silicas in less time and with good textural and physical-chemicals properties.

3.2 CO_2 adsorption

Figure 5 shows the CO_2 adsorption isotherms for the mesoporous silicas MCM-41 and SBA-15, carried out at temperatures of 0, 25, and 40 °C at a pressure of 1 bar. The adsorbents did not reach saturation, i.e, the maximum adsorption capacity under the conditions studied, however, it is believed that with greater time and pressure, these data would reach the maximum adsorption capacity. Silica SBA-15 has a greater capacity for adsorbing CO_2 than that of MCM-41. This happens because SBA-15 presents in its structure a greater amount of active sites available in the micropore region, being more prone to adsorb CO_2 [9]. Furthermore, with increasing temperature there is a decrease in the adsorption capacity of silica, for example, the SBA-MW60 adsorbs 2.16 mmol g^{-1} at 0 °C and decreases to 0.87 mmol g^{-1} at 40 °C, which suggests a weak interaction between the adsorbent and CO_2, as shown by the results found in the literature [27]. Amine groups are usually introduced on the surfaces of mesoporous silicas to improve the material's efficiency for CO_2 adsorption [1, 2, 35]. However, this study will also show that it is possible to obtain promising results, just by modifying the route of synthesis of ordered silicas without the insertion of amine groups.

It is noted that the tests performed at 0 °C showed the best results, showing adsorption capacities from 1.30 to 2.16 mmol g^{-1} at 1 bar. In addition, it is worth mentioning another important result, which was that the pure silicas obtained similarly and, in some cases, even superior to amine-modified silica. In the works of Muchan et al. [7], the synthesis of MCM-41 by the conventional method (24 h) was reported and they obtained a $Q_{ads} = 0.63$ mmol g^{-1}, while

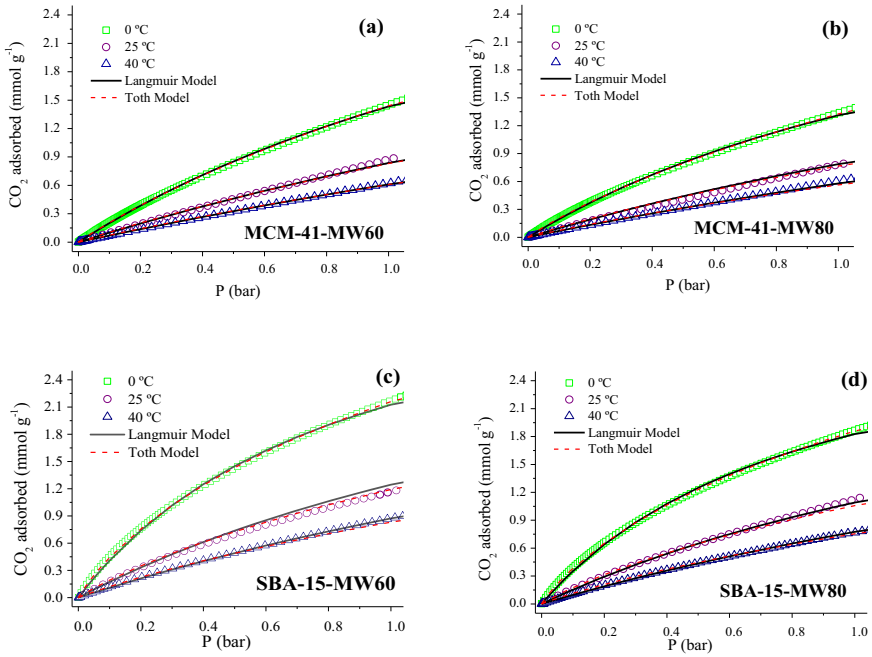

Fig. 5 CO_2 adsorption isotherms of the porous silicas MCM-41-MW60 (**a**), MCM-41-MW80 (**b**), SBA-15-MW60 (**c**) and SBA-15-MW80 (**d**). Solid lines for fit to Langmuir and dashed lines for Toth model

Table 2 Fit parameters for the CO_2 adsorption equilibrium isotherms for the Langmuir and Toth model on ordered mesoporous silicas

Langmuir				
Samples	q_m (mmol g^{-1})	b (bar^{-1})		$(-\Delta H)$ (kJ mol^{-1})
MCM-41-MW60	4.51	9.08×10^{-5}		19.4
MCM-41-MW80	3.58	1.08×10^{-4}		19.5
SBA-15-MW60	4.00	1.91×10^{-5}		25.0
SBA-15-MW80	3.41	2.56×10^{-5}		24.3
Toth				
Samples	q_m (mmol g^{-1})	b (bar^{-1})	ni	$(-\Delta H)$ (kJ mol^{-1})
MCM-41-MW60	9.49	4.77×10^{-5}	0.68	19.4
MCM-41-MW80	12.95	2.90×10^{-5}	0.53	20.0
SBA-15-MW60	8.79	6.52×10^{-6}	0.56	26.4
SBA-15-MW80	8.37	1.09×10^{-5}	0.53	25.1

Barbosa et al. [2] synthesized a silica MCM-41 by the conventional method (96 h) and modified with amine obtaining $Q_{ads} = 1.0$ mmol g^{-1}, at a temperature of 25 °C at 1 bar. In this work, with only 1 h of synthesis, it was possible to obtain a CO_2 adsorption capacity of $Q_{ads} = 0.88$ mmol g^{-1} at a temperature of 25 °C and 1 bar using the silicas synthesized in a MW reactor in a time of 1 h.

To fit the experimental data, the Langmuir and Toth models were applied, showing a good fit with the experimental data (Table 2). The model parameters were obtained for each silica, minimizing the sum of squares of the absolute errors between the calculated and experimental values with the help of the Solver supplement, in Excel, as well as in the work by Regufe et al. [8]. Both models show good agreement with the experimental data (Fig. 5) and can accurately predict the sites of CO_2 adsorption.

It can be seen in Table 2 that all silicas exhibit heat of adsorption between $\Delta H = -19.4$ and -26.4 kJ mol^{-1} for all models. These values agree with those reported in the literature, where lower heats of adsorption occur between -15 and -40 kJ mol^{-1}, being associated with poor adsorption due to physisorption processes [37, 38]. In all silicas, the adsorption process is favored at lower temperatures. The parameter n is related to the degree of surface homogeneity, with $n = 1$ for a completely smooth surface. The obtained values of n vary between 0.53 and 0.68 for the mesoporous silicas, showing heterogeneity of the CO_2 adsorption sites. The b values are related to the energetic interaction between the adsorbent and

Table 3 Bibliographic search of the amount of CO_2 adsorbed for silicas MCM-41 and SBA-15 compared with results obtained in this work

Adsorbent	Amine	T (°C)	S_{BET} ($m^2\ g^{-1}$)	Q_{ads} CO_2 (mmol g^{-1})	Reference
SBA-15	–	0	735	0.91	[35]
SBA-15	–		853	1.39	[52]
MCM-41	–		1168	1.43	
SBA-15-MW60	**–**		**788**	**2.16**	**This work**
SBA-15-MW80	**–**		**626**	**1.85**	
MCM-41-MW60	**–**		**999**	**1.44**	
MCM-41-MW80	**–**		**744**	**1.32**	
MCM-41	PEI		296	1.26	[52]
SBA-15			302	1.34	
SBA-15	–	25	665	0.64	[46]
	–		793	0.91	[53]
	–		735	0.53	[35]
MCM-41	–		1007	0.63	[7]
SBA-15-MW60	**–**		**788**	**1.18**	**This work**
SBA-15-MW80	**–**		**626**	**1.14**	
MCM-41-MW60	**–**		**999**	**0.88**	
MCM-41-MW80	**–**		**744**	**0.79**	
SBA-15	APTES		216	1.44	[47]
			389	1.37	[35]
MCM-41			665	1.00	[2]
SBA-15	PEI		49	1.33	[27]
MCM-41			24	3.53	[32]
SBA-15	–	30	572	0.59	[32]
			735	0.47	[35]
MCM-41	PEI		51	2.60	[54]
	–	40	985	0.25	
SBA-15-MW60	**–**		**788**	**0.87**	**This work**
SBA-15-MW80	**–**		**626**	**0.77**	
MCM-41-MW60	**–**		**999**	**0.62**	
MCM-41-MW80	**–**		**744**	**0.60**	

Bold values denote results obtained in this work

the adsorbate. The values obtained show a low interaction between CO_2 molecules [39]. The relative errors found in the experimental fit are between 1.2 and 3.6%, which indicates acceptable values. Therefore, the maximum CO_2 adsorption capacity of silica can be obtained using both models.

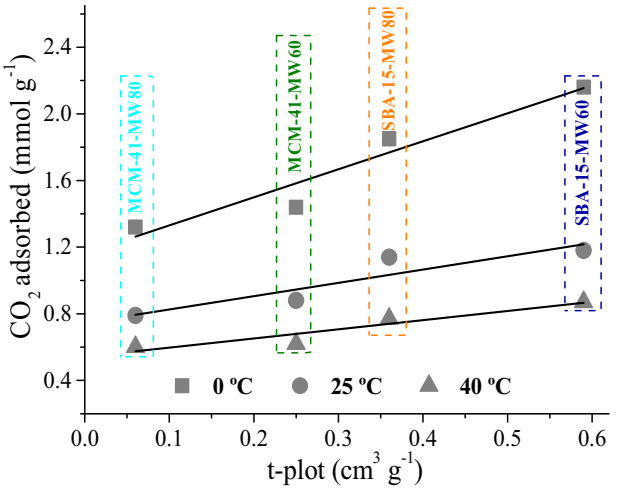

Fig. 6 Relationship between microporosity (t-plot) and CO_2 adsorption capacity of porous silicas (SBA-15 and MCM-41) under different CO_2 adsorption temperatures (0, 25 and 40 °C)

MCM-41 and SBA-15 silicas, in addition to their thermal and mechanical stability and high surface area, have silanol groups that allow greater interaction with other CO_2 molecules. Thus, the CO_2 adsorption results were satisfactory, as it was shown that it is possible to achieve good adsorption capacities at low temperature and pressure with pure silica, because in addition to impregnation with amine, the porous structure, the volume and diameter of pores, regeneration capacity and CO_2 selectivity are important factors to be analyzed [1, 7]. In addition, these results can still be more efficient by adjusting the experimental conditions of adsorption, since changes in temperature/pressure of adsorption affect the amount adsorbed [37]. Table 3 presents a bibliographic survey of similar studies using silicas of the MCM-41 and SBA-15 type, synthesized by the conventional hydrothermal method. It is noted that the adsorption capacity results obtained in this work were superior to those reported in similar studies using MCM-41 and SBA-15 silicas synthesized by the conventional hydrothermal method. In addition, it is worth mentioning another important result, which was that the pure silicas obtained similar adsorption capacities and, in some cases, even superior to amine-modified silicas.

Furthermore, it is worth adding that the adsorption capacity of CO_2 increases linearly according to microporosity (t-plot value) of the adsorbents, as shown in Fig. 6. The microporosity of silicas decreases with aging temperature increases. Galarneau et al. [31] have already reported similar results, where they showed that the use of lower aging temperature favors the interconnection of surfactant micelles (P123 or CTAB), in such a way that micropores are generated after calcination of the model. Thus, the silicas synthesized at 60 °C obtained micropores values higher than the silicas obtained at 80 °C, thus presenting better adsorption results.

Table 4 Thermodynamic parameters for CO_2 adsorption of the studied mesoporous silica

Samples	ΔH (kJ mol^{-1})	ΔS (J mol^{-1} K)	ΔG (kJ mol^{-1})			R_2
			0 °C	25 °C	40 °C	
MCM-41-MW60	14.44	49.86	0.802	−0.355	−1.217	0.9965
MCM-41-MW80	13.65	47.82	0.609	−0.636	−1.290	0.9988
SBA-15-MW60	14.61	47.85	1.561	0.307	−0.337	0.9986
SBA-15-MW80	13.77	45.82	1.224	0.225	−0.651	0.9899

3.3 Thermodynamic studies

The thermodynamic parameters (ΔH, ΔS and ΔG) for the prepared silica are given in Table 4. The values obtained for enthalpy variation (ΔH) indicate the nature of the adsorption process. Positive ΔH implies an endothermic nature, as was the case with the silicas used in this work (13.65 to 14.61 kJ mol^{-1}). The values of standard entropy variation (ΔS) were all positive for CO_2 adsorption, showing that during the entire adsorption process some structural changes occur on the silica surface [40]. The Gibbs free energy showed that increasing the adsorption temperature increases the negative value of ΔG, which consequently generates an increase in the degree of spontaneity for the adsorption of CO_2 in both adsorbents [40, 41]. The quantitative evaluation of these parameters requires a comparison of the correlation coefficients (R^2). Notably, the R^2 values calculated for the order parameters are greater than 0.98, thus indicating good linearization.

3.4 Stability of adsorbents

Practical applications in CO_2 capture demand robust adsorbents that exhibit thermal stability even after several adsorption/desorption cycles. To evaluate the regeneration capacity of the adsorbents, in Fig. 7, the silicas with the highest CO_2 adsorption capacity were chosen, in this case, MCM-41-MW60 and SBA-15-MW60. The reuse tests of these adsorbents during the three cycles are like each other, where changes hardly occur, indicating a similar adsorption capacity and good thermal stability. The silica SBA-15-MW60 and MCM-41-MW60 obtained CO_2 adsorption capacity of 1.16, 1.14, 1.12 mmol g^{-1} and 1.01, 1.0, 0.99 mmol g^{-1} in the 1st, 2nd and 3rd cycle, respectively. It is believed that the silicas would support more regeneration cycles since in the first runs there is a decrease in the adsorption capacity, however, the adsorbent reuse tests in three cycles succeeded in small decreases in the adsorbed amount of CO_2.

3.5 Amine influence

To evaluate the influence of the amine on the adsorption of CO_2, using silicas synthesized by microwave irradiation, the silica MCM-41-MW60 was chosen. N_2 and CO_2

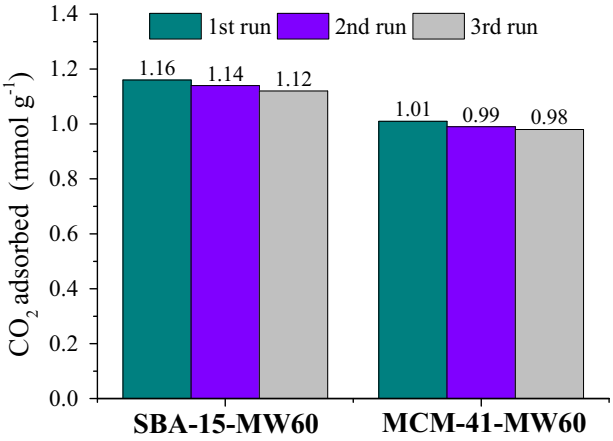

Fig. 7 CO_2 amount adsorbed for SBA-15-MW60 and MCM-41-MW60 at 25 °C and 1 bar for three runs

adsorption/desorption isotherms, CHN, FTIR, XPS, XRD, NMR, TEM analyses and morphology before and after PEI and TEPA impregnation were performed for MCM-41-MW60 silica and are presented below. It is worth remembering, the nomenclature used for modified silicas, where the letters P and T, are equivalent to the amine group PEI and TEPA, and the numbers 1, 2, 3 and 4, the amount of amine (25%, 40%, 55% and 70%) in mass, respectively.

Figure 8a shows that silicas of type MCM-41-MW60 impregnated with up to 55% amine continue to show Type IV isotherms with a hysteresis of type H4, even after impregnation. The MCM-41-MW60 isotherm showed two hysteresis loops: the first, shows a marked pore-filling step below the relative pressure of 0.45 and the second, a small step of N_2 adsorption in a P/P_0 range of 0.45–1.0, indicating a bimodal pore size distribution. When the amount of PEI or TEPA increases, the hysteresis loop became thinner or disappeared, indicating a decline in pore volume and specific surface area. According to Thommes et al. [29], this limiting adsorption is governed by the accessible micropore volume and not by the internal surface area. As this sample has the highest amount of amine, it is believed that PEI predominantly occupied the pore openings, thus hindering the entry of N_2 molecules [42].

Figure 8b shows some variations when the amine is impregnated on the silica surface through the pore size

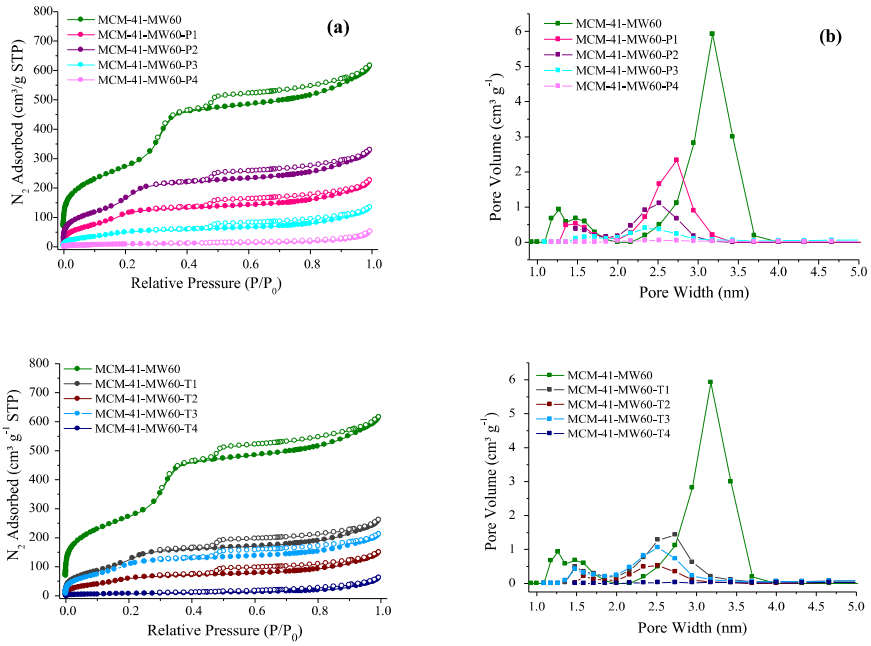

Fig. 8 N_2 adsorption/desorption isotherm at −196 °C (**a**) and pore size distribution determined by NLDFT method (**b**) of the MCM-41-MW60 modified with different amounts of PEI and TEPA

Table 5 Surface properties, elemental analysis, and adsorption capacity of CO_2 (Q_{ads}) obtained at 25 °C for the MCM-41-MW60 unmodified and modified mesoporous silicas

Samples	S_{BET} ($m^2\,g^{-1}$)	$S_{mp\ t\text{-}plot}$ ($m^2\,g^{-1}$)	Vp ($cm^3\,g^{-1}$)	$V_{mp\ t\text{-}plot}$ ($cm^3\,g^{-1}$)	Dp_{DFT} (nm)	C (%)	H (%)	N (%)	Q_{ads} (mmol g^{-1})
MCM-41-MW60	999	780	0.89	0.59	3.71	0.22	1.25	0.0	0.88
MCM-41-MW60-P1	563	442	0.46	0.27	2.73	9.07	2.18	5.1	0.98
MCM-41-MW60-P2	378	288	0.30	0.15	2.53	13.23	2.99	7.6	1.30
MCM-41-MW60-P3	194	127	0.17	0.05	2.35	16.06	3.86	9.65	1.54
MCM-41-MW60-P4	33	13	0.04	0.005	–	21.15	5.32	11.8	0.46
MCM-41-MW60-T1	552	451	0.35	0.19	2.75	8.81	4.25	5.9	1.83
MCM-41-MW60-T2	360	195	0.19	0.07	2.52	14.22	4.97	8.8	1.90
MCM-41-MW60-T3	458	352	0.29	0.13	2.51	17.45	4.54	10.9	2.10
MCM-41-MW60-T4	27	–	0.06	–	–	18.75	4.91	11.4	1.33

distribution. For MCM-41-MW60 we have a wider pore distribution and as the amount of amine impregnated increases, the pore distribution becomes narrower, and the adsorbed volume is much smaller. However, MCM-41-MW60-P4 and MCM-41-MW60-T4 does not have the same properties due to saturated pores from excess amine, which corroborates the great extent of PEI or TEPA modification in silica pores.

The structural characteristics of this sample are shown in Table 5. Because of filling the pores with PEI/TEPA, the surface area and the pore volume decreased according to the amount of amine impregnated, which can be correlated with the values obtained by the CHN elemental analysis, since the higher the percentage of C and N, the smaller the surface area and pore volume. These results have already been reported in several studies, for example, Sanz-Perez et al. [37] synthesized SBA-15 and impregnated it with 30% TEPA, reporting a decrease in surface area from 720 to 128 $m^2\,g^{-1}$. Rao et al. [32] synthesized silica MCM-41 and impregnated with 50% PEI, reporting a decrease in surface area from 998 to 24 $m^2\,g^{-1}$. Cecilia et al. [27] impregnated 50% PEI onto SBA-15 silica and reported a decrease in surface area from 665 to 19 $m^2\,g^{-1}$.

In Fig. 9, the FTIR spectra show the characteristic peaks of SiO_2 where it is possible to observe the groups that form the chemical structure of these materials. FTIR spectra of the TEPA-impregnated MCM-41 silicas present similar bands to those of the PEI-impregnated samples (Fig. 9a). The bands at 810 and 1074 cm^{-1} are observed in all samples, characteristic of the bending vibration and asymmetric stretching of the Si-O-Si group [43]. For amine-impregnated silicas, new bands appear when compared to that of the MCM-41-MW60. A very important bond to confirm the

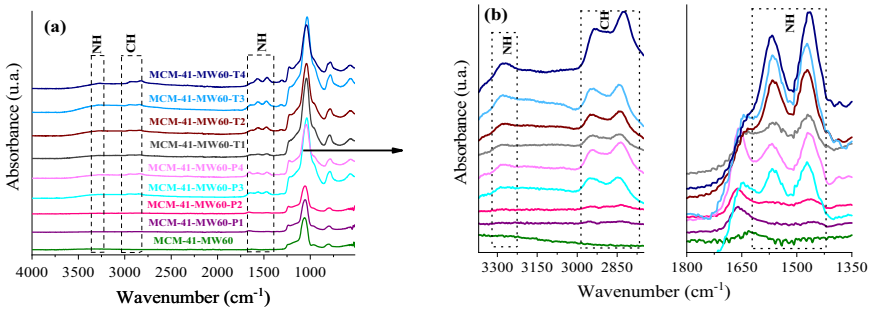

Fig. 9 FTIR spectra (**a**) and zoom of bands NH and CH (**b**) for the MCM-41-MW60 and MCM-41-MW60 impregnated with PEI and TEPA

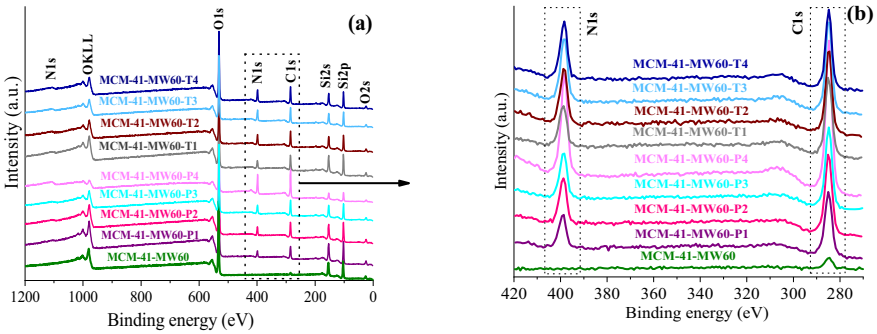

Fig. 10 XPS survey spectra (**a**) and zoom of signals N1s and C1s (**b**) for the MCM-41-MW60 and MCM-41-MW60 impregnated with PEI and TEPA

modification with PEI and TEPA is the N-H bond, referring to the amine groups (–NH_2).

In Fig. 9b this functional group is observed in the form of symmetrical angular deformation in the region of around 1565 and 1485 cm^{-1} and the stretching band N-H in the region of 3300 cm^{-1} [1, 13]. Note that the greater the amount of amine impregnated in the silica, the greater the intensity of the band, which is not very noticeable for samples impregnated with 25% PEI or TEPA. The two bands located at 2955 and 2825 cm^{-1}, which are more visible for silicas impregnated with 55 and 70% amine, are attributed to asymmetric and symmetrical C H stretching vibrations [44]. The band in the region of 960 cm^{-1} is attributed to the Si-OH stretch, however, in the modified silica, it is not possible to visualize this band due to the amount of PEI or TEPA impregnated on the silica surface, since the amine groups interact with most of the hydroxyl groups (OH) [13, 35]. In addition to the FTIR analysis, it was possible to confirm the modification of the surface of the silica, through XPS (Fig. 10a). Amine-modified MCM-41 silicas show signals from C 1*s*, N 1*s*, Si 2*p* and O 1*s*, where it is also noted that the N and C signals increase according to the amount of PEI or TEPA impregnated on the surface increases (Fig. 10b). The results obtained through the XPS, corroborate the data obtained by the CHN elemental analysis, where we can see that the atomic concentration of the elements increases according to the amount of amine impregnated (Table 6).

Table 6 Atomic concentration determined by XPS for the MCM-41-MW60 and MCM-41-MW60 modified with PEI and TEPA

Samples	XPS—Atomic concentration (%)			
	C 1*s*	N 1*s*	O 1*s*	Si 2*p*
MCM-41-MW60-P1	17.88	5.93	54.57	21.62
MCM-41-MW60-P2	23.10	8.41	48.74	19.76
MCM-41-MW60-P3	26.27	10.00	46.01	17.72
MCM-41-MW60-P4	46.42	19.73	24.48	9.37
MCM-41-MW60-T1	20.63	7.55	51.00	20.83
MCM-41-MW60-T2	25.35	11.57	44.52	18.56
MCM-41-MW60-T3	25.54	12.16	45.2	17.10
MCM-41-MW60-T4	27.22	12.60	42.25	17.93

The confirmation of the hexagonal structure of the silicas and to verify if there was any change in the structure after impregnation with amine was done by using the TEM and X-ray diffraction technique. According to the images provided by the TEM, it is evident the visualization of the ordered mesoporous silica MCM-41 particles, even after impregnation with PEI (Fig. 11a) or TEPA (Fig. 11b), shows that a material synthesized by MW also obtains good results for a modified surface. The transmission microscopy presents materials with hexagonal channels with long-range two-dimensional ordering and images in the direction perpendicular to the pore axis, revealing the set of channels that make up this silica. The XRD pattern of silicas (Supplementary Material—Fig. 14) present only

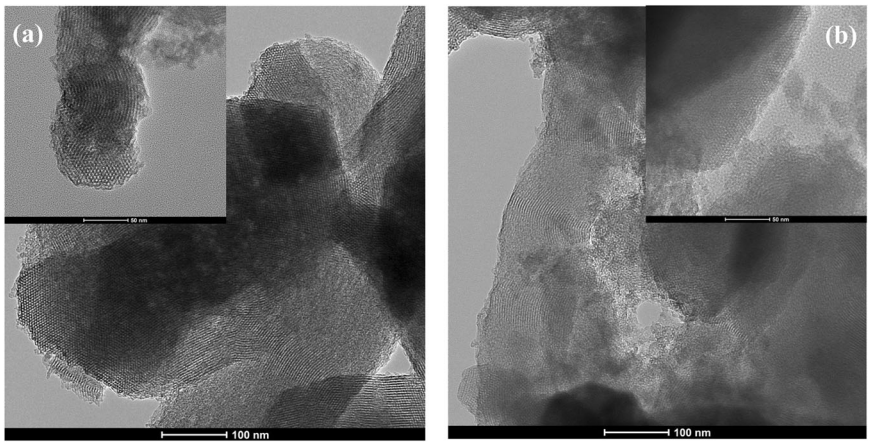

Fig. 11 Transmission electron microscopy was obtained at 50 and 100 nm of the mesoporous silicas **a** MCM-41-MW60-P2 and **b** MCM-41-MW60-T2

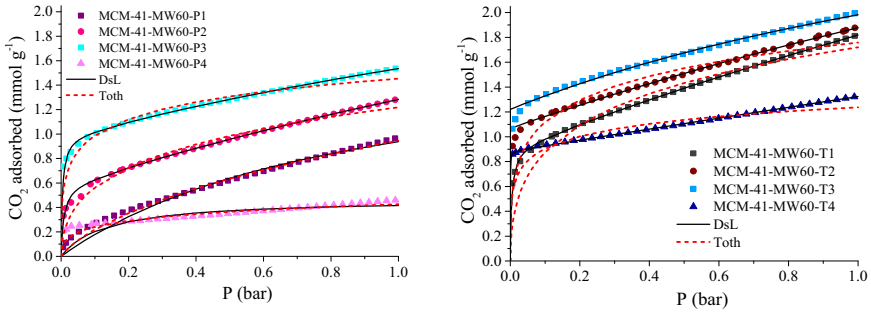

Fig. 12 CO_2 adsorption isotherms at 25 °C of the porous modified silicas with amine. Solid lines for fit to DsL model, and dashed lines red Toth model

the main peak referring to the (100) plane, which characterizes ordered mesoporous materials. The peaks of the modified silicas were shifted toward the upper angle when compared to MCM-41-MW60 and the peak intensity decreased or even disappeared, which was consistent with the amount of PEI or TEPA on the surface of the silica, thus indicating a greater occupation of the pores. Sanz-Pérez et al. [45] reported that the reduction in diffraction peak intensity with TEPA and PEI impregnation is due to pore filling with organic compounds that prevent X-ray diffraction through the mesoporous structure. This suggests that the gradual reduction in peak intensity of the amine-modified MCM-41 is due to pore filling with PEI or TEPA, thus corroborating the results discussed above. However, this shift and the weaker peaks do not compromise the formation of the ordered silica network and agree with the results described in the literature, where this shift of the diffraction peak was also reported [2, 16, 32]. Moreover, the TEM images of MCM-41, confirm an ordered structure of the material, with a regular hexagonal array of mesoporous channels.

To better understand the performance of pure and PEI/TEPA-modified MCM-41-MW60 in CO_2 adsorption, adsorption tests were performed at 25 °C up to 1 bar. The results are shown in Fig. 12. The CO_2 adsorption isotherms of the PEI-modified silicas showed a steep initial slope at pressures below 0.1 bar, followed by a slight smooth increase in the amount of CO_2 adsorbed. This behavior can be associated with the chemical reaction between CO_2 and the amine groups, which present a greater interaction [1]. Many studies have also reported that the increase in the CO_2 adsorptive capacity of materials containing greater amounts of amine can be attributed to interactions of hydrogen bonds between hydrogen atoms (of NH) and CO_2 molecules [1, 37, 46].

It is noted that the adsorption capacity of MCM-41-MW60 increases according to the amount of PEI impregnated, being 0.98 and 1.54 mmol g^{-1} for MCM-MW60-P1 and MCM-41-MW60-P3, respectively. There was an increase in the amount adsorbed for the TEPA-modified silicas when we analyzed the results obtained by PEI, with the adsorption capacity of MCM-41-MW60-T1 and MCM-41-MW60-T3 being 1.83 mmol and 2.10 mmol g^{-1}, respectively. This improvement occurs because TEPA is a polymer that has a lower viscosity than PEI, thus reducing the clustering of amine groups and favoring greater interaction with CO_2 molecules, thus favoring the adsorption process [37]. However, for samples MCM-41-MW60-P4 and MCM-41-MW60-T4, there was a sudden drop in adsorption capacity, to 0.47 and 1.33 mmol g^{-1},

Table 7 Fit parameters for the CO_2 for the DsL and Toth model on PEI and TEPA impregnated silicas

Dualsite Langmuir					
Samples	q_{m1} (mmol g^{-1})	b_1 (bar^{-1})	q_{m2} (mmol g^{-1})	b_2 (bar^{-1})	$(-\Delta H)_1$ (kJ mol^{-1})
MCM-41-MW60-P1	1.77	6.23×10^{-8}	1.46	3.31×10^{-9}	41.4
MCM-41-MW60-P2	0.60	1.18×10^{-6}	4.43	1.60×10^{-7}	46.1
MCM-41-MW60-P3	0.98	9.93×10^{-9}	2.76	2.44×10^{-9}	59.5
MCM-41-MW60-P4	0.47	1.04×10^{-8}	0.44	2.34×10^{-9}	50.6
MCM-41-MW60-T1	0.91	6.30×10^{-9}	7.34	5.25×10^{-9}	60.5
MCM-41-MW60-T2	1.07	1.21×10^{-6}	4.92	1.36×10^{-7}	62.8
MCM-41-MW60-T3	2.33	1.51×10^{-8}	1.22	2.65×10^{-9}	42.8
MCM-41-MW60-T4	0.88	1.33×10^{-8}	18.72	2.65×10^{-9}	66.2

Toth				
Samples	q_m (mmol g^{-1})	b (bar^{-1})	n_i	$(-\Delta H)$ (kJ mol^{-1})
MCM-41-MW60-P1	11.77	1.82×10^{-5}	0.32	25.5
MCM-41-MW60-P2	9.45	1.66×10^{-5}	0.18	38.8
MCM-41-MW60-P3	4.36	1.84×10^{-5}	0.15	57.5
MCM-41-MW60-P4	2.41	1.83×10^{-5}	0.14	49.1
MCM-41-MW60-T1	8.27	1.13×10^{-5}	0.18	42.9
MCM-41-MW60-T2	7.77	3.01×10^{-5}	0.13	55.8
MCM-41-MW60-T3	8.32	1.32×10^{-5}	0.11	67.2
MCM-41-MW60-T4	2.94	1.83×10^{-5}	0.14	61.7

respectively, where the amine probably blocked the silica pores, making the interaction with CO_2 difficult.

The CO_2 adsorption process on porous silica occurs predominantly by physisorption, where the silica acts as a molecular sieve for CO_2 molecules, limiting the affinity with CO_2 compared to the adsorption process governed by chemisorption [13]. Nevertheless, the impregnation of amine groups leads to the adsorption of CO_2 occurring through physisorption and chemisorption. Thus, the DsL model, which assumes the coexistence of both adsorption sites, was used to predict the fit of these data. Table 7 confirms the coexistence of both types of sites, although the affinity of CO_2 for chemical sites is higher, as suggested by the values of parameter b, we can also confirm the presence of physisorption sites [47, 48].

In general, good adjustments were obtained, referring to the applied models (Fig. 12). The Langmuir model is the most widely used expression for physical monolayer adsorption and chemisorption, and the Toth model is an empirical model that was developed to produce a better fit when compared to the models presented above. Based on the results obtained here, it is noted that the greatest increase in CO_2 adsorption capacity occurred when comparing the MCM-41-MW60 ($Q_{ads} = 0.88$ mmol g^{-1}—Fig. 5) with the MCM-41-MW60-T3 ($Q_{ads} = 2.10$ mmol g^{-1}—Fig. 12). Although amine-modified MCM-41 absorbs more CO_2 than MCM-41-MW60, we can see that pure silicas show promising results. In addition, the modification of the silica surface with the amine group, as well as the chemical and thermal stability, suggest that the hydrophilicity/hydrophobicity of the adsorbent is altered, which can generate a greater interaction with CO_2, leading to an increase in the adsorption capacity [49, 50]. These results are the result of a balance between the textural parameters of the silicas and the functional characteristics of each amine [51].

It is noteworthy that it was also possible to obtain good results for CO_2 adsorption using pure silica synthesized by MW. This happens because silicas synthesized by MW have a greater amount of silanol groups than silicas synthesized by the hydrothermal method in an autoclave, making the adsorbents more hydrophilic and consequently a greater number of active sites available for CO_2 adsorption [16]. It is also noted that the synthesis process per MW is different from the conventional heating methodology, wherein MW irradiation it is possible to generate an accelerated crystallization rate in a short time, in the case of ordered silica synthesis, possibly the mesoporous structure and ordering of the particles will be generated in the initial minutes, where the microwaves are being transmitted at higher power. Thus, the synthesis of MCM-41 and SBA-15 per MW can be efficiently used in the CO_2 adsorption process.

4 Conclusions

Silicas of MCM-41 and SBA-15 types were synthesized in 1 h at 60 and 80 °C with good quality and thermal stability. Microwave irradiation-assisted synthesis showed a significant reduction in time and energy consumption compared to conventional autoclave synthesis, without modifying the structural and morphological characteristics of the materials, proving to be an efficient synthesis for ordered mesoporous materials.

The pure silicas synthesized in microwaves (1 h) present similar results to silicas synthesized in autoclave (20–96 h) modified with amine for CO_2 adsorption, thus confirming the efficiency of this method, which in addition to reducing the synthesis time, can also dispense with the use of amine modification/impregnation methodologies. The CO_2 adsorption isotherms showed that the adsorption capacity of silicas decreases with increasing temperature and the most promising adsorbent in terms of adsorption capacity is SBA-15 reaching a CO_2 adsorption capacity of 2.16 mmol g^{-1} at 1 bar and 0 °C.

The MCM-41 silicas modified with PEI and TEPA improved the CO_2 adsorption capacity, which increased from 0.88 mmol g^{-1} to 1.5 and 2.1 mmol g^{-1} at 1 bar and 25 °C, respectively. All the silicas obtained in this study (unmodified or modified) can be applied in CO_2 adsorption processes, due to their textural and morphological, physicochemical properties and good stability.

Acknowledgements We also thank Servicio Central de Apoyo a la Investigación (SCAI—Universidad de Málaga) for analysis.

Author contributions MRO: investigation, methodology, formal analysis, writing—original draft preparation, validation; JFC: conceptualization, supervision, writing—review and editing; JAC: conceptualization, validation, writing; SME: conceptualization, supervision, project administration; ER-C: writing—review, conceptualization, supervision, project administration, funding acquisition. All authors have read and agreed to the published version of the manuscript.

Funding The authors thank you to Conselho Nacional de Desenvolvimento Científico e Tecnológico (CNPq, National Council for Scientific and Technological Development, Brazil) and Coordenação de Aperfeiçoamento de Pessoal de Nível Superior (Higher Education Personnel Improvement Coordination, Brazil, CAPES—financing code 001) for financial support. This research was also funded by the Ministry of Science, Innovation and Universities (Spain), Grants Nos. RTI2018-099668-B-C22 and PID2021-126235OB-C32, and projects UMA18-FEDERJA-126 and P20_00375 of Junta de Andalucía and FEDER funds. Funding for open access publishing: Universidad Málaga/CBUA.

Compliance with ethical standards

Conflict of interest The authors declare no competing interests.

References

1. Oliveira RJ, Oliveira MR, De Conto JF, Borges GR, Dariva C, Egues SM, Franceschi E (2019) CO_2/CH_4 adsorption at high-pressure using silica-APTES aerogel as adsorbent and near infrared as a monitoring technique. J CO_2 Util 32:232–240. https://doi.org/10.1016/j.jcou.2019.04.019
2. Barbosa MN, Costa MJF, Barbosa MN, Fernandes Júnior VJ, Salazar-Banda GR, Reyes-Carmona Á, Rodríguez-Castellón E, Araujo AS (2021) Aminopropyltriethoxysilane functionalized MCM-41 and SBA-15 nanostructured materials for carbon dioxide adsorption. Rev Mat. https://doi.org/10.1590/S1517-707620210004.1385
3. Watabe T, Yogo K (2013) Isotherms and isosteric heats of adsorption for CO_2 in amine-functionalized mesoporous silicas. Sep Purif Technol. https://doi.org/10.1016/j.seppur.2013.09.011
4. Zhang G, Zhao P, Hao L, Xu Y (2018) Amine-modified SBA-15(P): a promising adsorbent for CO_2 capture. J CO_2 Util. https://doi.org/10.1016/j.jcou.2017.12.006
5. Santos KMC, Menezes TR, Oliveira MR, Silva TSL, Santos KS, Barros VA, Melo DC, Ramos AL, Santana CC, Franceschi E, Dariva C, Egues SM, Borges GR, De Conto JF (2021) Natural gas dehydration by adsorption using MOFs and silicas: a review. Sep Purif Technol. https://doi.org/10.1016/j.seppur.2021.119409
6. Nascimento RF, Lima ACA, Vidal CB, Melo DQ, Raulino GSC (2014) Adsorção: Aspectos teóricos e aplicações ambientais. Fortaleza-CE, Brasil
7. Muchan P, Saiwan C, Nithitanakul M (2020) Investigation of adsorption/desorption performance by aminopropyltriethoxysilane grafted onto different mesoporous silica for post-combustion CO_2 capture. Clean Energy 4:120–131. https://doi.org/10.1093/ce/zkaa003
8. Regufe MJ, Ferreira AFP, Loureiro JM, Rodrigues A, Ribeiro AM (2019) Electrical conductive 3D-printed monolith adsorbent for CO_2 capture. Micropor Mesopor Mat. https://doi.org/10.1016/j.micromeso.2019.01.009
9. Vilarrasa-García E, Cecilia JA, Moura PAS, Azevedo DCS, Rodríguez-Castellon E (2020) Assessing CO_2 adsorption on amino-functionalized mesocellular foams synthesized at different aging temperatures. Front Chem. https://doi.org/10.3389/fchem.2020.591766
10. Hughes R, Kotamreddy G, Ostace A, Bhattacharyya D, Siegelman RL, Parker ST, Didas SA, Long JR, Omell B, Matuszewski M (2021) Isotherm, kinetic, process modeling, and techno-economic analysis of a diamine-appended metal−organic framework for CO_2 capture using fixed bed contactors. Energy Fuels 35:6040–6055. https://doi.org/10.1021/acs.energyfuels.0c04359

11. Beck JS, Vartuli JC, Roth WJ, Leonowicz ME, Kresge CT, Schmitt KD, Chu CTW, Olson DH, Sheppard EW, Mccullen SB, Higgins JB, Schlenkert JL (1992) A new family of mesoporous molecular sieves prepared with liquid crystal templates. J Am Chem Soc 114:10834–10843. https://doi.org/10.1021/ja00053a020
12. Zhao DY, Feng JL, Huo QS, Melosh N, Fredrickson GH, Chmelka BF, Stucky GD (1998) Triblock copolymer syntheses of mesoporous silica with periodic 50 to 300 angstrom pores. Science 279:548–52. https://doi.org/10.1126/science.279.5350.548
13. Cecilia JA, Vilarrasa-García E, García-Sancho C, Saboya RMA, Azevedo DCS, Cavalcante Jr CL, Rodríguez-Castellón E (2016) Functionalization of hollow silica microspheres by impregnation or grafted of amine groups for the CO_2 capture. Int J Greenh Gas Control 52:344–356. https://doi.org/10.1016/j.ijggc.2016.07.018
14. Tan X, Huang Z, Jiang L, Xiao T, Wang Y, Yang X, Zhu H, Li S, Chen X (2021) A simple fabrication of superhydrophobic PVDF/SiO_2 coatings and their anti-icing properties. J Mater Res 36:637–645. https://doi.org/10.1557/s43578-020-00034-z
15. Oliveira MR, Oliveira MM, Oliveira RJ, Dervanoski A, Franceschi E, Egues SM, De Conto JF (2019) Amine-modified silica surface applied as adsorbent in the phenol adsorption assisted by ultrasound. Chem Eng Commun 206:1554–1569. https://doi.org/10.1080/00986445.2019.1615467
16. Oliveira MR, Deon M, Benvenutti EV, Barros VA, Melo DC, Franceschi E, Egues SM, De Conto JF (2020) Effect of microwave irradiation on the structural, chemical, and hydrophilicity characteristics of ordered mesoporous silica SBA-15. J Sol-Gel Sci Technol 94:708–718. https://doi.org/10.1007/s10971-020-05219-w
17. Furukawa H, Gandara F, Zhang YB, Jiang J, Queen WL, Hudson MR, Yaghi OM (2014) Water adsorption in porous metal−organic frameworks and related materials. J Am Chem Soc 136:4369–81. https://doi.org/10.1021/ja500330a
18. Mayanovic RA, Yan H, Brandt AD, Wang Z, Mandal M, Landskron K, Bassett WA (2014) Mechanical and hydrothermal stability of mesoporous materials at extreme conditions. Micropor Mesopor Mater 195:161–166. https://doi.org/10.1016/j.micromeso.2014.04.027
19. De Conto JF, Oliveira M, Oliveira RJ, Campos KV, De Menezes EW, Benvenutti EV, Franceschi E, Santana CC, Egues SM (2017) Synthesis of silica modified with 1-methylimidazolium chloride by sol-gel method: a comparison between microwave radiation-assisted and conventional methods. J Non-Cryst Solids 471:209–214. https://doi.org/10.1016/j.jnoncrysol.2017.05.041
20. Peres EC, Slaviero JC, Cunha AM, Hosseini–Bandegharaei A, Dotto GLJ (2018) Microwave synthesis of silica nanoparticles and its application for methylene blue adsorption. Environ Chem Eng 6:649–659. https://doi.org/10.1016/j.jece.2017.12.062
21. Bordoni AV, Lombardo MV, Wolosiuk A (2021) Rapid pore expansion of mesoporous silica-based materials using microwave irradiation and pore swelling agents. Mater Chem Phys 274:125185. https://doi.org/10.1016/j.matchemphys.2021.125185
22. You H-S, Jin H, Mo Y-H, Park S-E (2013) CO_2 adsorption behavior of microwave synthesized zeolite beta. Mater Lett 108:106–109. https://doi.org/10.1016/j.matlet.2013.06.088
23. Rueda M, Sanz-Moral LM, Nieto-Márquez A, Longone P, Mattea F, Martín A (2014) Production of silica aerogel microparticles loaded with ammonia borane by batch and semicontinuous supercritical drying techniques. J Supercrit Fluid 92:299–310. https://doi.org/10.1016/j.supflu.2014.06.012
24. Greñu BD, De los Reyes R, Costero AM, Amorós P, Ros-Lis JV (2020) Recent progress of microwave-assisted synthesis of silica materials. Nanomaterials 10. https://doi.org/10.3390/nano10061092
25. Grun M, Unger KK, Matsumoto A, Tsutsumi K (1999) Novel pathways for the preparation of mesoporous MCM-41 materials: control of porosity and morphology. Micropor Mesopor Mat 27:207–216. https://doi.org/10.1016/S1387-1811(98)00255-8
26. Xu X, Song C, Andrésen JM, Miller BG, Scaroni AW (2003) Preparation and characterization of novel CO_2 "molecular basket" adsorbents based on polymer-modified mesoporous molecular sieve MCM-41. Micropor Mesopor Mater 62:29–45. https://doi.org/10.1016/S1387-1811(03)00388-3
27. Cecilia JA, Vilarrasa-García E, Morales-Ospino R, Bastos-Neto M, Azevedo DCS, Rodríguez-Castellón E (2020) Insights into CO_2 adsorption in amino-functionalized SBA-15 synthesized at different aging temperature. Adsorption 26:225–240. https://doi.org/10.1007/s10450-019-00118-1
28. Do DD (1998) Adsorption analysis: equilibria and kinetics. Imperial College Press, London
29. Thommes M, Kaneko K, Neimark AV, Olivier JP, Rodriguez-Reinoso F, Rouquerol J, Sing KSW (2015) Physisorption of gases, with special reference to the evaluation of surface area and pore size distribution (IUPAC Technical Report). Pure Appl Chem 87:1051–1069. https://doi.org/10.1515/pac-2014-1117
30. Santos BF, Cecilia JA, Bastos-Neto M, Rodríguez-Castellón E, Azevedo DCS, Vilarrasa-García E (2022) Insights into optimized synthesis conditions of hollow microspheres of silica for water vapor adsorption. Chem Eng Res Des 177:583–593. https://doi.org/10.1016/j.cherd.2021.11.020
31. Galarneau A, Cambon H, Di Renzo F, Fajula F (2001) True microporosity and surface area of mesoporous SBA-15 silicas as a function of synthesis temperature. Langmuir 17:8328–8335. https://doi.org/10.1021/la0105477
32. Rao N, Wang M, Shang Z, Hou Y, Fan G, Li J (2018) CO_2 adsorption by amine-functionalized MCM-41: a comparison between impregnation and grafting modification methods. Energy Fuels 32:670–677. https://doi.org/10.1021/acs.energyfuels.7b02906
33. Yamashita T, Hayes P (2008) Analysis of XPS spectra of Fe^{2+} and Fe^{3+} ions oxide. Appl Surf Sci 254:2441–2449. https://doi.org/10.1016/j.apsusc.2007.09.063
34. Sales RV, Moura HOMA, Câmara ABF, Rodríguez-Castellón E, Silva JAB, Pergher SBC, Campos LMA, Urbina MM, Bicudo TC, Carvalho LS (2019) Assessment of Ag nanoparticles interaction over low-cost mesoporous silica in deep desulfurization of diesel. Catalysts 9:651. https://doi.org/10.3390/catal9080651
35. Ojeda-López R, Domínguez-Ortiz A, Felipe C, Cervantes-Uribe A, Pérez-Hermosillo IJ, Esparza-Schulz JM (2021) Adsorption on micro-mesoporous materials: carbon microfibers (CMFs), SBA-15, and amine-functionalized SBA-15. J Compos Sci 5:102. https://doi.org/10.3390/jcs5040102
36. Chaignon J, Bouizi Y, Davin L, Calin N, Albela B, Bonneviot L (2015) Minute-made and low carbon fingerprint microwave synthesis of high quality templated mesoporous silica. Green Chem 17:3130–3140. https://doi.org/10.1039/C5GC00038F
37. Sanz-Pérez ES, Arencibia A, Sanz R, Calleja G (2016) New developments on carbon dioxide capture using amine-impregnated silicas. Adsorption 22:609–619. https://doi.org/10.1007/s10450-015-9740-2
38. Samanta A, Zhao A, Shimizu GKH, Sarkar P, Gupta R (2012) Post-combustion CO_2 capture using solid sorbents: a review. Ind Eng Chem Res 51:1438–1463. https://doi.org/10.1021/ie200686q
39. Candamano S, Policicchio A, Conte G, Abarca R, Algieri C, Chakraborty S, Curcio S, Calabró V, Crea F, Agostino RG (2022) Preparation of foamed and unfoamed geopolymer/NaX zeolite/activated carbon composites for CO_2 adsorption. J Clean Prod 330:129843. https://doi.org/10.1016/j.jclepro.2021.129843
40. Kumar A, Rout S, Ghosh M, Singhal RK, Rav PM (2013) Thermodynamic parameters of U (VI) sorption onto soils in aquatic systems. Springerplus 2:530. https://doi.org/10.1186/2193-1801-2-530

41. Humelnicu D, Zinicovscaia I, Humelnicu I, Ignat M, Yushin N, Grozdov D (2022) Study on the SBA-15 silica and ETS-10 titanosilicate as efficient adsorbents for Cu (II) removal from aqueous solution. Water 14:857. https://doi.org/10.3390/w14060857
42. Ma J, Liu Q, Chen D, Wen S, Wang T (2014) CO_2 adsorption on amine-modified mesoporous silicas. J Porous Mat 21:859–867. https://doi.org/10.1007/s10934-014-9835-2
43. Yang G, Deng Y, Ding H, Lin Z, Shao Y, Wang Y (2015) A facile approach to synthesize MCM-41 mesoporous materials from iron ore tailing: Influence of the synthesis conditions on the structural properties. Appl Clay Sci 111:61–66. https://doi.org/10.1016/j.clay.2015.04.005
44. Drage TC, Arenillas A, Smith KM, Snape CE (2008) Thermal stability of polyethylenimine based carbon dioxide adsorbents and its influence on selection of regeneration strategies. Micro Mesop Mater 116:504–512. https://doi.org/10.1016/j.micromeso.2008.05.009
45. Sanz-Peŕez ES, Olivares-Marín M, Arencibia A, Sanz R, Calleja G, Maroto-Valer MM (2013) CO_2 adsorption performance of amino-functionalized SBA-15 under post-combustion conditions. Int J Greenh Gas Control 17:366–375. https://doi.org/10.1016/j.ijggc.2013.05.011
46. Sánchez-Vicente Y, Stevens LA, Pando C, Torralvo MJ, Snape CE, Drage TC, Cabañas A (2015) A new sustainable route in supercritical CO_2 to functionalize silica SBA-15 with 3-aminopropyltrimethoxysilane as material for carbon capture. Chem Eng J 264:886–898. https://doi.org/10.1016/j.cej.2014.12.002
47. Vilarrasa-García E, Cecilia JA, Moya EMO, Cavalcante Jr CL, Azevedo DCS, Rodríguez-Castellón E (2015) "Low Cost" pore expanded SBA-15 functionalized with amine groups applied to CO_2 adsorption. Materials 8:2495–2513. https://doi.org/10.3390/ma8052495
48. De Sousa JAR, Amâncio R, Morales-Ospino R, De Oliveira JLB, Cecilia JÁ, Vilarrasa-García E, Bastos-Neto M, Rodríguez-Castellón E, De Azevedo DCS (2021) H_2S and H_2O combined effect on CO_2 capture by amino functionalized hollow microsphere silicas. Ind Eng Chem Res 60:10139–10154. https://doi.org/10.1021/acs.iecr.1c00033
49. Liu Y, Tan X, Li X, Xiao T, Jiang L, Nie S, Song J, Chen X (2022) Eco-friendly fabrication of transparent superhydrophobic coating with excellent mechanical robustness, chemical stability, and long-term outdoor durability. Langmuir 38:12881–12893. https://doi.org/10.1021/acs.langmuir.2c01998
50. Tan X, Wang Y, Huang Z, Sabin S, Xiao T, Jiang L, Chen X (2021) Facile fabrication of a mechanical, chemical, thermal, and long-term outdoor durable fluorine-free superhydrophobic coating. Adv Mater Interfaces. https://doi.org/10.1002/admi.202002209
51. Tumurbaatar O, Lazarova H, Popova M, Mitova V, Shestakova P (2022) CO_2 adsorption on the N- and P-modified mesoporous silicas. Nanomaterials 12. https://doi.org/10.3390/nano12071224
52. Yan X, Komarneni S, Yan Z (2013) CO_2 adsorption on Santa Barbara Amorphous-15 (SBA-15) and amine-modified Santa Barbara Amorphous-15 (SBA-15) with and without controlled microporosity. J Colloid Interface Sci 390:217–24. https://doi.org/10.1016/j.jcis.2012.09.038
53. Munguía-Cortés L, Pérez-Hermosillo I, Ojeda-López R, Esparza-Schulz JM, Felipe-Mendoza C, Cervantes-Uribe A, Domínguez-Ortiz A (2017) APTES-functionalization of SBA-15 using ethanol or toluene: textural, characterization and sorption performance of carbon dioxide. J Mexican Chem Soc 61. https://doi.org/10.29356/jmcs.v61i4.457
54. Le MUT, Seul-Yi L, Park S-J (2014) Preparation and characterization of PEI-loaded MCM-41 for CO_2 capture. Int J Hydrog Energy 39:12340–12346. https://doi.org/10.1016/j.ijhydene.2014.04.112